Phenyl-pyta-tricarbonylrhenium(I) complexes: Combining a simplified structure and steric hindrance to modulate the photoluminescence properties

Alexandre Poirot, Corinne Vanucci-Bacqué, Béatrice Delavaux-Nicot, Nadine Leygue, Nathalie Saffon-Merceron, Fabienne Alary, Florence Bedos-Belval, Eric Benoist and Suzanne Fery-Forgues*

Infrared spectroscopy

Crystallographic data

Electrochemistry

Quantum chemistry calculations

Photochemistry

Emission spectroscopy

Fluorescence microscopy

NMR

Infrared spectroscopy

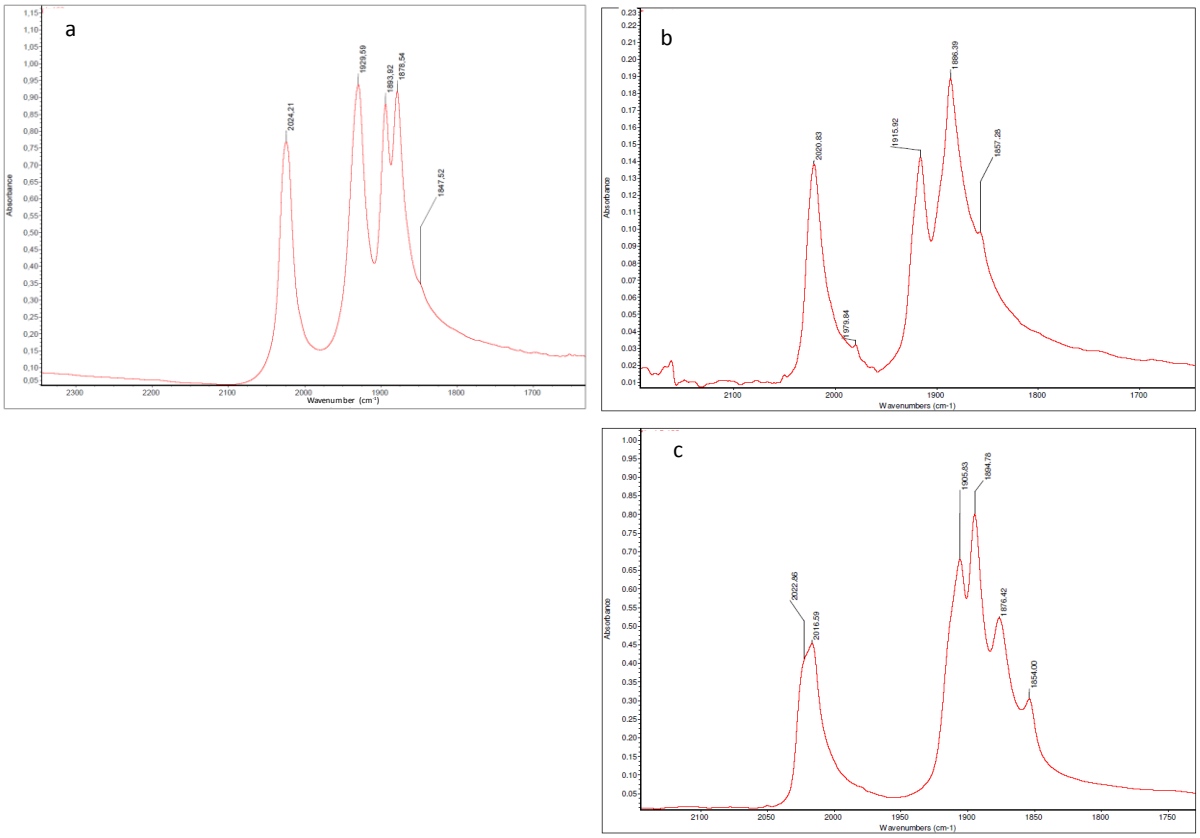

Figure S1. ATR IR spectra of complexes **1** (a), **2** (b) and **3** (c). The sample of **1** was a powder dispersed in KBr. Samples of **2** and **3** were as-prepared microcrystalline powders.

Crystallographic data

Table S1. Selected bond lengths (Å) for complexes **1**-**3**. Data related to the second molecule of the asymmetric unit of **1** are mentioned in blue ink. The atoms were numbered like on the molecular views. For the sake of comparison, each line corresponds to the same bond in every complex.

Bond	**1**	**2**	**Bond**	**3**
Re1-Cl1/Re2-Cl2	2.474(2)/2.476(2)	2.4766(8)	Re1-Cl1	2.4712(7)
Re1-N1/Re2-N5	2.200(7)/2.191(7)	2.202(3)	Re1-N1	2.204(2)
Re1-N2/Re2-N6	2.147(7)/2.157(8)	2.153(2)	Re1-N2	2.147(2)
Re1-C1/Re2-C17	1.935(10)/1.899(10)	1.921(3)	Re1-C1	1.908(3)
Re1-C2/Re2-C18	1.902(11)/1.900(10)	1.917(4)	Re1-C3	1.914(3)
Re1-C3/Re2-C19	1.869(10)/1.895(10)	1.908(4)	Re1-C2	1.916(3)
O1-C1/O4-C17	1.140(11)/1.150(10)	1.144(4)	O1-C1	1.156(4)
O2-C2/O5-C18	1.171(11)/1.148(10)	1.147(4)	O3-C3	1.147(4)
O3-C3/O6-C19	1.182(10)/1.159(10)	1.147(4)	O2-C2	1.144(4)

Table S2. Selected angles (°) for complexes **1**-**3**. Data related to the second molecule of the asymmetric unit of **1** are mentioned in blue ink. The atoms were numbered like on the molecular views. For the sake of comparison, each line corresponds to the same bond in each complex.

Bond angles	**1**	**2**	**Bond angles**	**3**
C3-Re1-C2/C19-Re2-C18	89.0(4)/89.5(4)	89.67(15)	C2-Re1-C3	88.85(15)
C3-Re1-C1/C19-Re2-C17	89.5(4)/87.0(4)	88.16(15)	C2-Re1-C1	87.74(14)
C2-Re1-C1/C18-Re2-C17	90.1(4)/89.3(4)	88.16(14)	C3-Re1-C1	88.80(14)
C3-Re1-N2/C19-Re2-N6	97.2(3)/96.7(3)	96.32(12)	C2-Re1-N2	97.59(12)
C2-Re1-N2/C18-Re2-N6	98.1(3)/99.1(3)	98.37(12)	C3-Re1-N2	98.37(12)
C1-Re1-N2/C17-Re2-N6	169.5(3)/170.8(3)	172.08(12)	C1-Re1-N2	171.12(12)
C3-Re1-N1/C19-Re2-N5	93.0(3)/93.9(3)	93.70(13)	C2-Re1-N1	93.98(12)
C2-Re1-N1/C18-Re2-N5	171.9(3)/173.1(3)	171.87(12)	C3-Re1-N1	172.05(11)
C1-Re1-N1/C17-Re2-N5	97.7(3)/97.0(3)	99.33(12)	C1-Re1-N1	98.73(11)
N2-Re1-N1/N6-Re2-N5	73.9(3)/74.5(3)	73.92(10)	N2-Re1-N1	73.91(9)
C3-Re1-Cl1/C19-Re2-Cl2	176.5(3)/177.1(3)	176.99(10)	C2-Re1-Cl1	178.49(11)
C2-Re1-Cl1/C18-Re2-Cl2	94.5(3)/93.5(3)	93.04(11)	C3-Re1-Cl1	92.66(11)
C1-Re1-Cl1/C17-Re2-Cl2	90.7(3)/92.9(3)	93.23(11)	C1-Re1-Cl1	92.30(10)
N2-Re1-Cl1/N6-Re2-Cl2	82.09(18)/82.94(18)	82.00(7)	N2-Re1-Cl1	82.19(7)
N1-Re1-Cl1/N5-Re2-Cl2	83.53(19)/83.23(18)	83.44(7)	N1-Re1-Cl1	84.53(6)
O1-C1-Re1/O4-C17-Re2	178.3(9)/176.4(9)	178.5(3)	O1-C1-Re1	178.8(3)
O2-C2-Re1/O5-C18-Re2	177.5(9)/179.7(9)	178.5(3)	O3-C3-Re1	177.7(3)
O3-C3-Re1/O6-C19-Re2	177.1(8)/176.7(8)	177.9(3)	O2-C2-Re1	178.7(4)

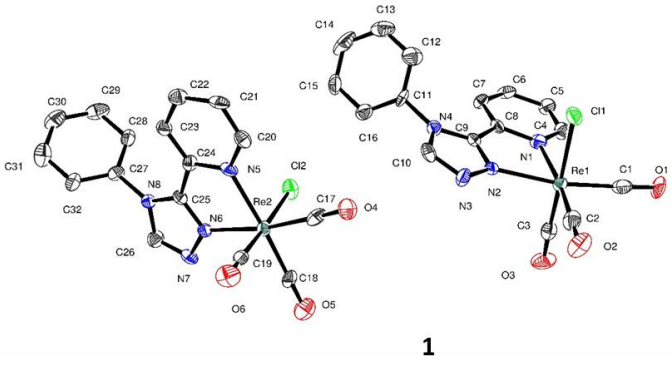

1

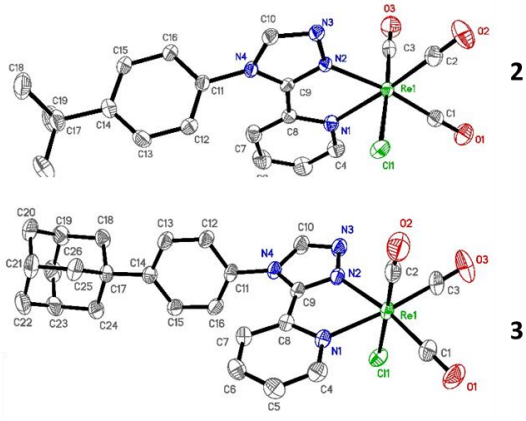

2

3

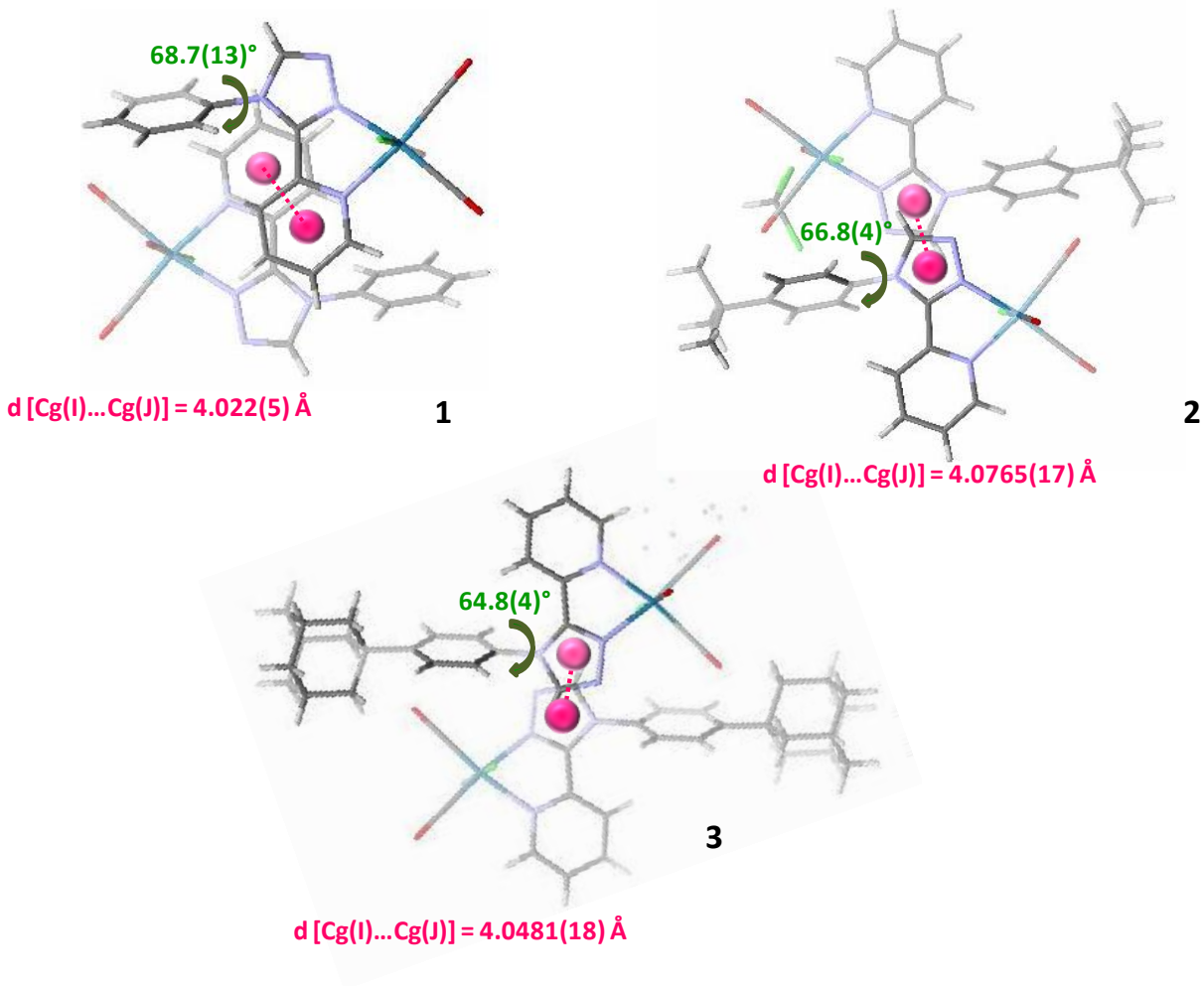

Figure S2. Crystallographic arrangement of complexes **1**, **2** and **3**. The values of the dihedral pyta-phenyl angle are indicated with green ink. View perpendicular to the plane formed by the pyta moieties, showing the absence of overlaps between the aromatic moieties of neighbouring molecules I and J. The distances between the ring center-of-gravity Cg indicated by pink balls are the shortest ones.

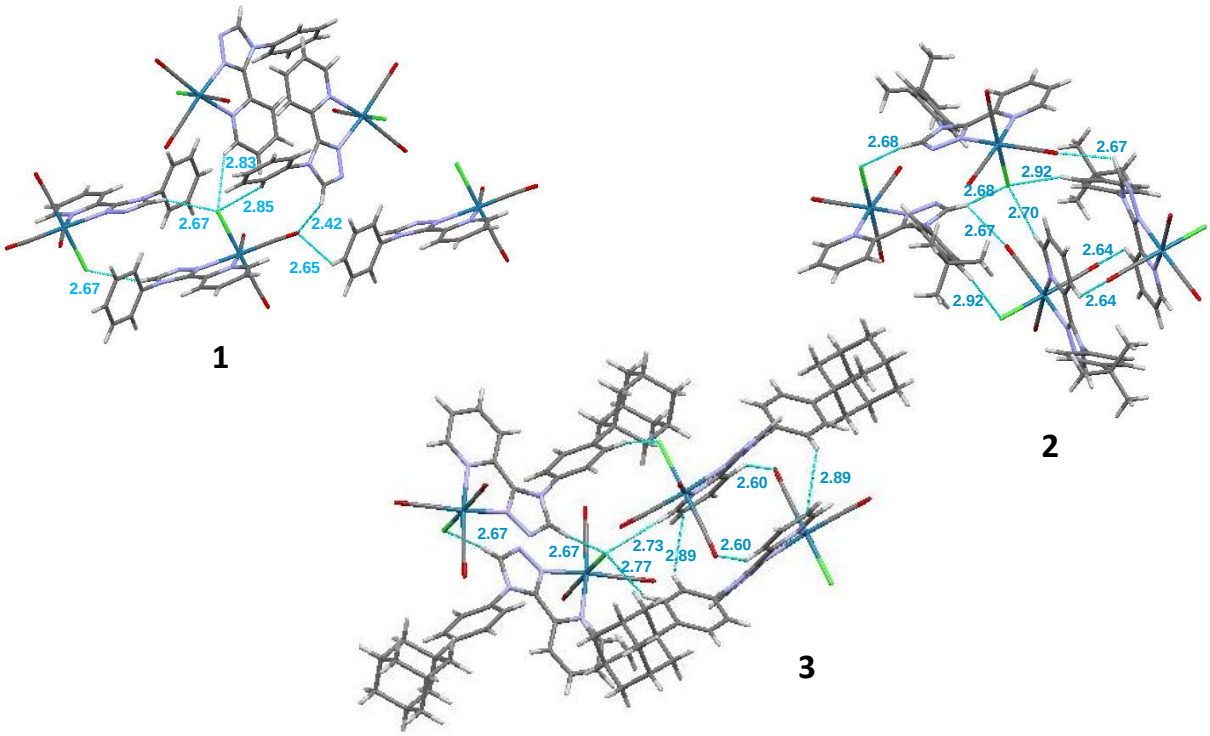

Figure S3. Short contacts (in Å) in complexes **1**, **2** and **3**.

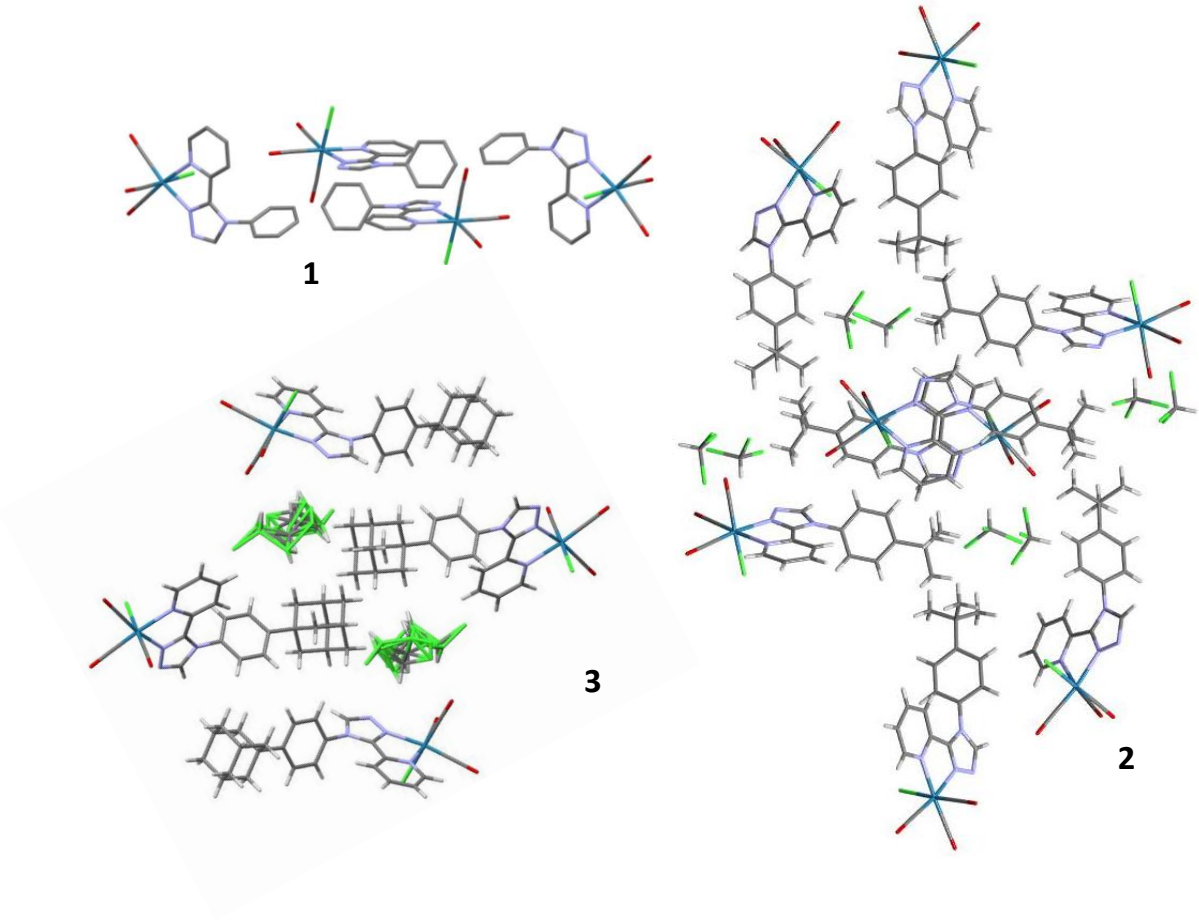

Figure S4. Crystal cell units of complexes **1**, **2** and **3**.

Electrochemistry

Table S3. Selected electrochemical data of Re complexes [1.0 × 10^{-3} M]. Values determined by OSWV on a Pt working electrode in CH_2Cl_2 + 0.1 M *n*-Bu_4NBF_4 at room temperature.[a,b] Ferrocene was used as internal reference**.**

Compound	Oxidation		Reduction		
	E_2	E_1	E_1	E_2[e]	E_3
1	1.78	1.46	–1.29[d]	–1.78	
2	1.81	1.49[c]	–1.28[d]	–1.89	
3	1.78	1.46[c]	–1.33[d]	–1.78	
RePBO[h]	1.73	1.44	–1.28[f]	–1.58	–1.83[g]

[a] OSWVs were obtained using a sweep width of 20 mV, a frequency of 20 Hz, and a step potential of 5 mV.
[b] Potential values in Volts vs. SCE (Fc^+/Fc is observed at 0.55 V ± 0.01 V *vs.* SCE).
[c] This process presents some slightly reversible character at 50 V/s.
[d] One-electron quasi-reversible process at 1.0 V/s.
[e] This process has a weak intensity when compared to the E_1 reduction process or appears as a shoulder.
[f] Quasi-reversible process at 0.2 V/s.
[g] With a shoulder at the right side
[h] From J. Wang, A. Poirot, B. Delavaux-Nicot, M. Wolff, S. Mallet-Ladeira, J. P. Calupitan, C. Allain, E. Benoist and S. Fery-Forgues, *Dalton Trans*., **2019**, *48*, 15906–15916.

Table S4. Experimental electrochemical data used, and calculated values of the energy gaps (*Eg*) for compounds **1**-**3**.

Compound	E_{onset} ox (V)	E_{onset} red (V)	E_{HOMO} (eV)	E_{LUMO} (eV)	E_g^{el} (eV)	E_{calc} [a] (eV)
1	1.42	–1.23	–6.16	–3.51	2.65	2.73
2	1.40	–1.22	–6.14	–3.52	2.62	2.74
3	1.41	–1.24	–6.15	–3.50	2.65	2.74
RePBO	1.34	–1.16	–6.08	–3.58	2.50	2.73 2.65 [b]

[a] When not specified, values obtained from theoretical study in the present work, using TD-DFT method and considering the S_1 state.
[b] Value obtained in a previous work using another procedure: (*Dalton Trans*., **2019**, *48*, 15906–15916).

Comments on the evaluation of the energy gap values (E_g) for the Re complexes.

The onset oxidation and reduction potentials (E_{onset} ox, E_{onset} red) were measured by cyclic voltammetry in volt *versus* SCE. The CVs were carried out at a potential scan rate of 200 mV s^{-1} at room temperature.

The HOMO and LUMO energy levels (E_{HOMO} and E_{LUMO}) in electron volt (eV) were calculated according to the empirical equations (1) and (2): [1]

E_{HOMO} (eV) = -e (E_{onset} ox (V vs. SCE) + 4.74 V) *Eq(1)*

E_{LUMO} (eV) = -e (E_{onset} red (V vs. SCE) + 4.74 V) *Eq(2)*

and the energy gap value was obtained as follows: $E_g^{el} = (E_{LUMO} - E_{HOMO})$.

The differences observed for the estimation of the energy gaps using experimental methods or theoretical calculations are well known. See for example: R. Stowasser, R. Hoffmann, *J. Am. Chem. Soc.* **1999**, *121*, 3414-3420.

[1] a) Y. Zhou, J. W. Kim, R. Nandhakumar, M. J. Kim, E. Cho, Y. S. Kim, Y. H. Jang, C. Lee, S. Han, K. M. Kim, J.-J. Kim and J. Yoon, *Chem. Commun.* **2010**, *46*, 6512-6514 and references therein; b) G. V. Loukova, *Chem. Phys. Lett.* **2002**, *353*, 244–252

Electrochemical selected curves

OSWV study was performed on a Pt working electrode in CH_2Cl_2 + 0.1 M *n*[Bu_4N][BF_4] at room temperature in the presence of ferrocene used as internal reference. Frequency 20 Hz, amplitude 20 mV, step potential 5 mV.

Cyclic voltammograms of the indicated compounds were performed on a Pt working electrode in CH_2Cl_2 + 0.1 M *n*[Bu_4N][BF_4] at room temperature at a scan rate of 0.2 Vs^{-1} or at other mentioned scan rates.

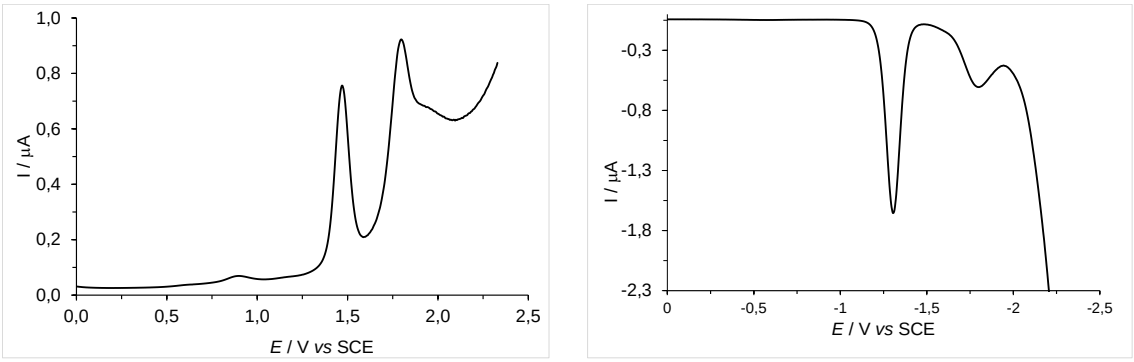

Figure S5. OSWVs: anodic (left) and cathodic (right) scans of complex **1**.

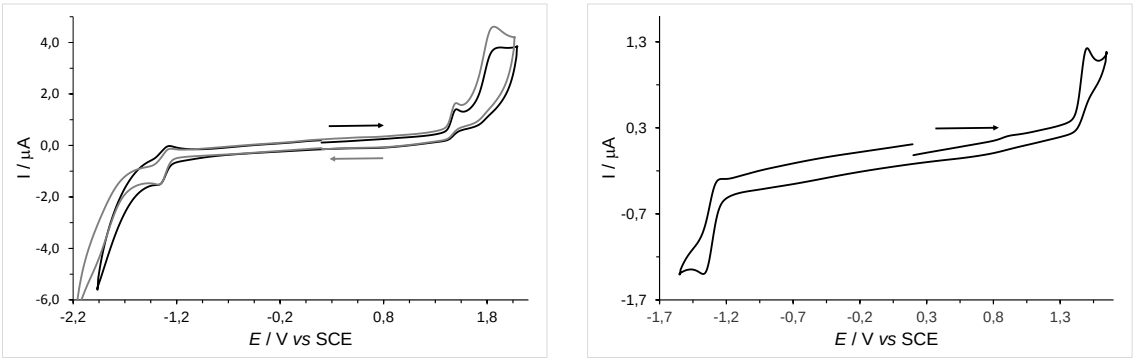

Figure S6. Cyclic voltammograms of complex **1** (left), and of its first oxidation and reduction processes (right).

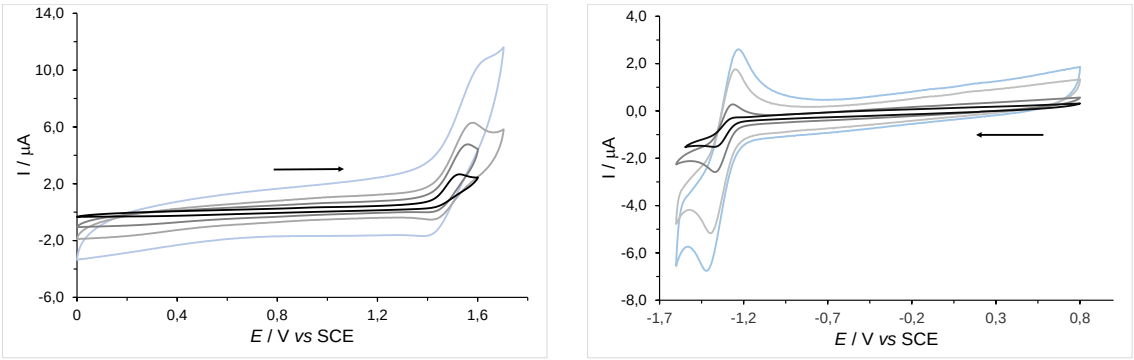

Figure S7. Complex **1**: Cyclic voltammograms of the first oxidation process at 1, 5, 10, 20 V/s from bottom to top (left), and of the first reduction process at 0.2, 1, 5, 10 V/s from bottom-black line to top-blue line (right).

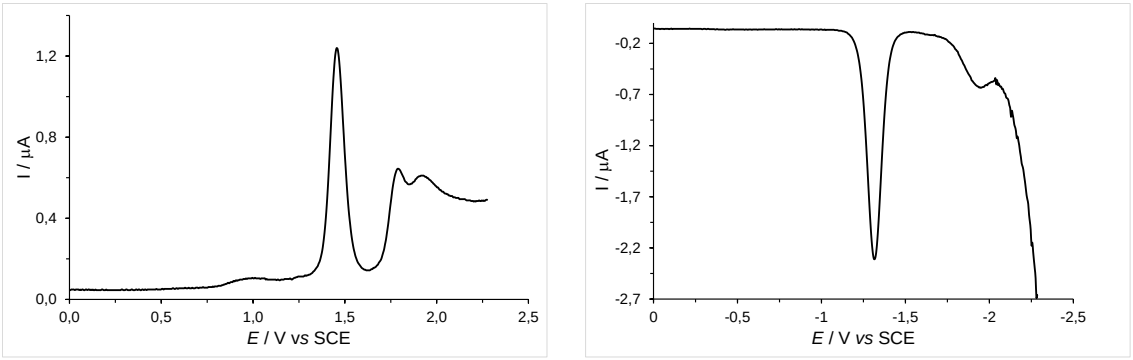

Figure S8. OSWVs: anodic (left) and cathodic (right) scans of complex **2**.

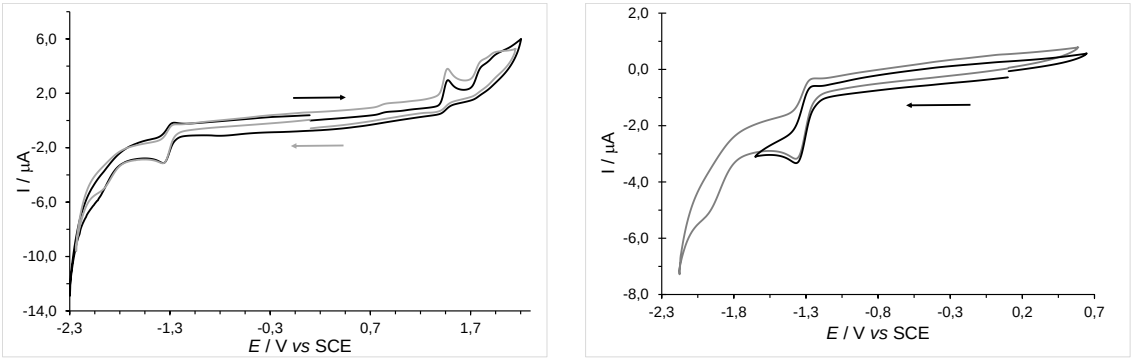

Figure S9. Cyclic voltammograms of complex **2** (left), and of its reduction processes at increasing potential (right).

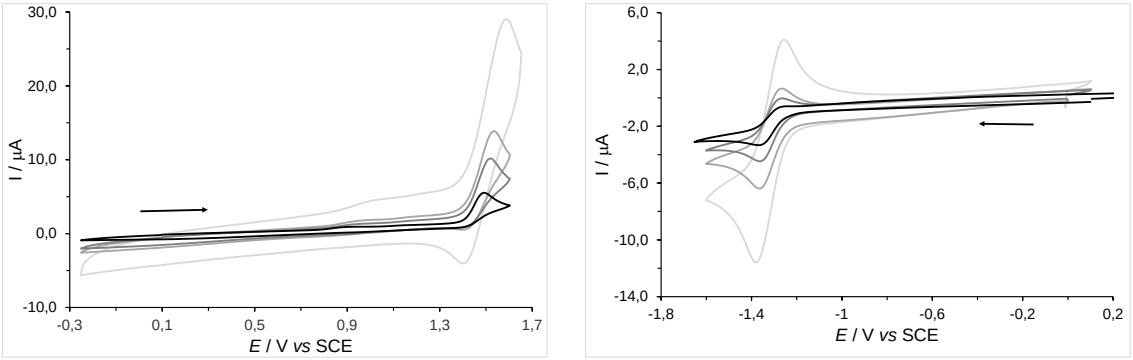

Figure S10. Complex **2**: Cyclic voltammograms of the first oxidation process at 1, 5, 10, 50 V/s from bottom-black line to top-grey line (left) and of the first reduction process at 0.2, 0.5, 1, 5 V/s from bottom-black line to top-grey line (right).

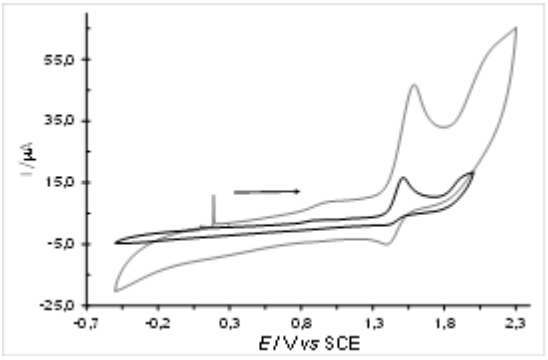

Figure S11. Cyclic voltammograms of the oxidation processes of complex **2** at 5 V/s (black line), and 50 V/s (grey line).

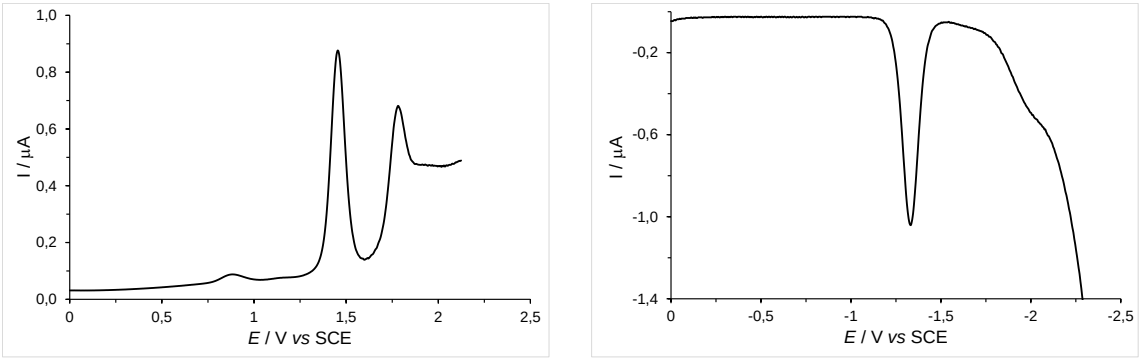

Figure S12. OSWVs: anodic (left) and cathodic (right) scans of complex **3**.

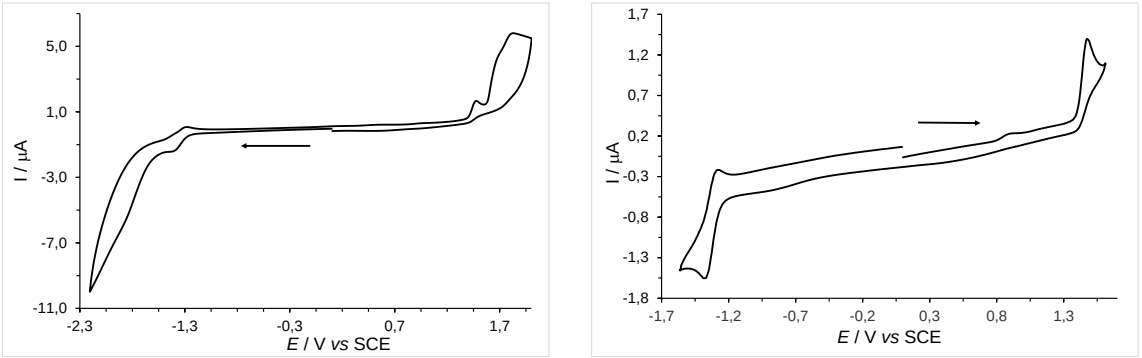

Figure S13. Cyclic voltammograms of complex **3** (left), and of its first oxidation and reduction processes (right).

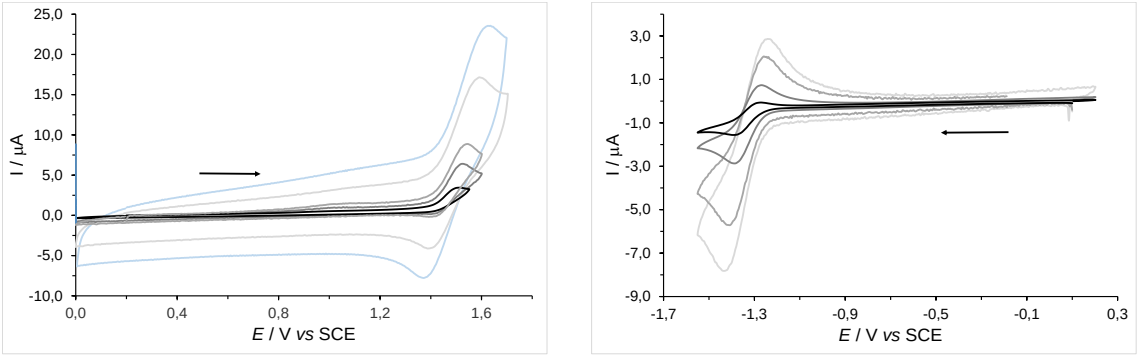

Figure S14. Complex **3**: Cyclic voltammograms of the first oxidation process at 1, 5, 10, 50 and 100 V/s from bottom-black line to top-blue line (left), and of the first reduction process at 0.2, 1, 5, 10 V/s from bottom-black line to top-grey line (right).

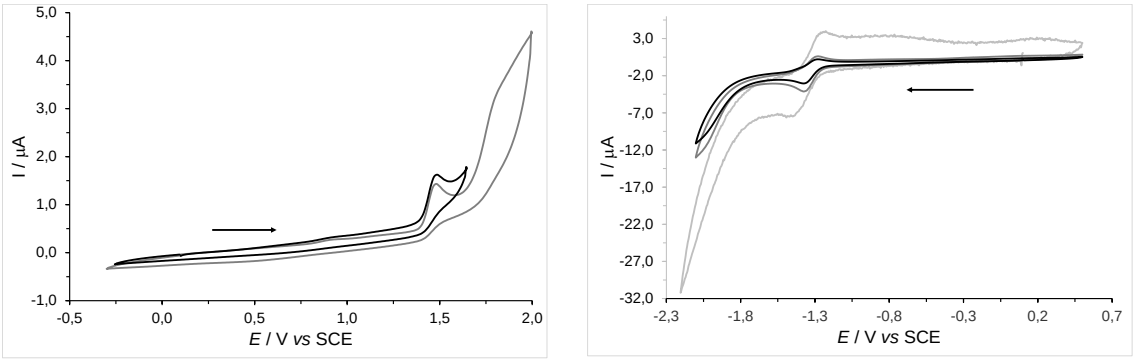

Figure S15. Complex **3**: Cyclic voltammograms of the oxidation part at increasing potential and of the reduction part at 0.5, 1, and 5 V/s from bottom-black line to top-light grey-line (right).

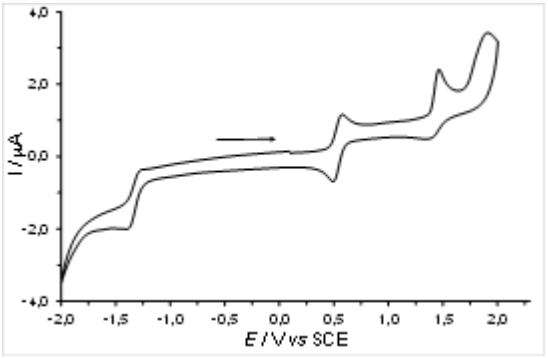

Figure S16. Cyclic voltammogram of complex **3** in the presence of ferrocene.

Quantum chemistry calculations

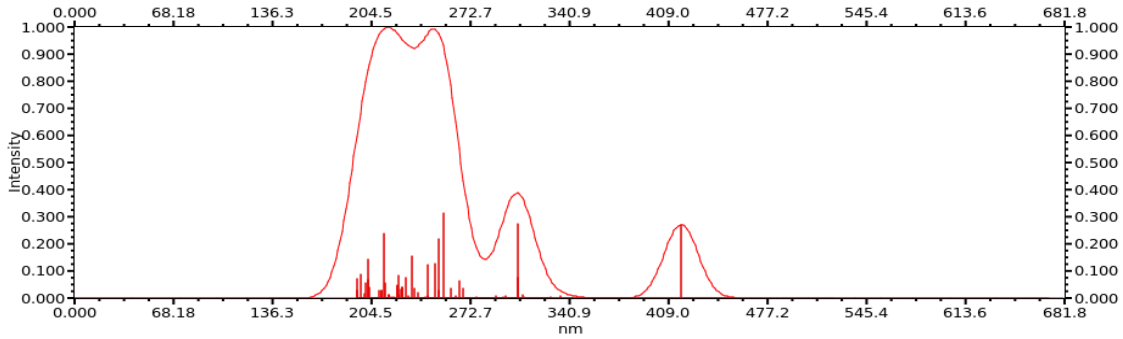

Figure S17. Theoretical UV-vis absorption spectrum and main electronic transitions for complex **1** in CH_2Cl_2 calculated using the TD-DFT method at the PBEO/LANL2DZ level.

Table S5. Description of the main electronic transitions for complex **1** in CH_2Cl_2 calculated using the TD-DFT method at the PBEO/LANL2DZ level, with corresponding wavelength (λ), energy (E) and oscillator strength (f).

Electronic transition	Contribution	Assignment		λ (nm)	E (eV)	f
$S_0 \rightarrow S_2$	H-1→LUMO	p(Cl)+ π(CO)+d(Re)→ π*(Pyta)+p(Re)+ π*(CO)	MLCT	418.2	2.97	0.0919
$S_0 \rightarrow S_{10}$	H-4→LUMO H-5→LUMO	p(Cl)+d(Re)+π(Phe)→ π*(Pyta)+p(Re)+ π*(CO) π(Phe)+p(Cl)+d(Re)→ π*(Pyta)+p(Re)+ π*(CO)	MLCT/LLCT LLCT	305.3	4.06	0.0925
$S_0 \rightarrow S_{20}$	H-7→LUMO	p(Cl)+d(Re)+π(Pyta) → π*(Pyta)+p(Re)+ π*(CO)	MLCT	254.2	4.88	0.1057
$S_0 \rightarrow S_{21}$	H-2→L+2 H-1→L+7 H-7→LUMO	d(Re)+π(CO)+p(Cl) → p(Re)+ π*(CO)+π*(Phe) p(Cl)+ π(CO)+d(Re) → π*(CO)+π*(Pyta) p(Cl)+d(Re)+π(Pyta) → π*(Pyta)+p(Re)+ π*(CO)	MLCT MLCT LLCT	251.4	4.93	0.0742
$S_0 \rightarrow S_{21}$	H-3→L+1	p(Cl)+d(Re)+π(Pyta)→π*(Pyta)	LLCT/MLCT	248.8	4.98	0.0435
$S_0 \rightarrow S_{24}$	H-1→L+5 H-8→LUMO	p(Cl)+π(CO)+d(Re)→ π*(Phe)+π*(Pyta)+p(Re)+π*(CO) p(Cl)+d(Re) → π*(Pyta)+p(Re)+π*(CO)	LLCT LLCT	243.4	5.09	0.0424
$S_0 \rightarrow S_{30}$	H-5→L+1	π(Phe)+p(Cl)+d(Re)→π*(Pyta)	ILCT/LLCT/ MLCT	232.7	5.33	0.0522
$S_0 \rightarrow S_{48}$	H-1→L+10 H-3→L+4	p(Cl)+ π(CO)+d(Re) → p(Re)+ π*(CO)+π*(Pyta) p(Cl)+d(Re)+π(Pyta) → p(Re)+ π*(CO)+π*(Phe)	LLCT LLCT	213.2	5.82	0.0799
$S_0 \rightarrow S_{54}$	H-13→LUMO H-2→L+10	π(CO)+π(Pyta) → π*(Pyta)+p(Re)+ π*(CO) d(Re)+π(CO)+p(Cl) → p(Re)+ π*(CO)+π*(Pyta)	LLCT LLCT	202.7	6.12	0.0488
$S_0 \rightarrow S_{58}$	H-11→LUMO	π(Pyta) → π*(Pyta)+p(Re)+ π*(CO)	LMCT	197.1	6.29	0.0300

Photochemistry

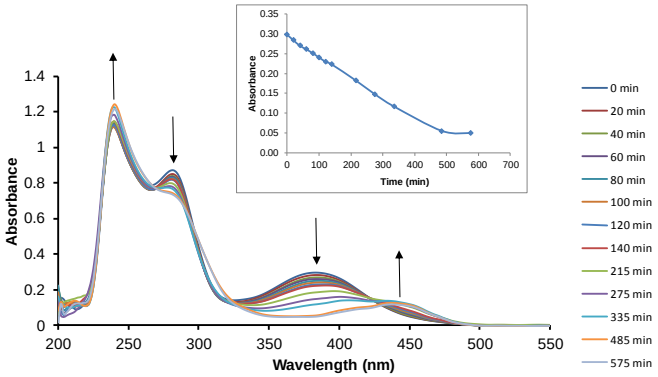

Figure S18. Evolution of the UV-vis absorption spectrum of **1** in undegassed dichloromethane solution (7.5×10^{-5} M) under irradiation at 350 nm over almost 9h30. Photolysis is achieved at 485 min (~8h). Arrows indicate the evolution of absorbance. Inset: Variation of absorbance at 382 nm as a function of time.

Emission spectroscopy

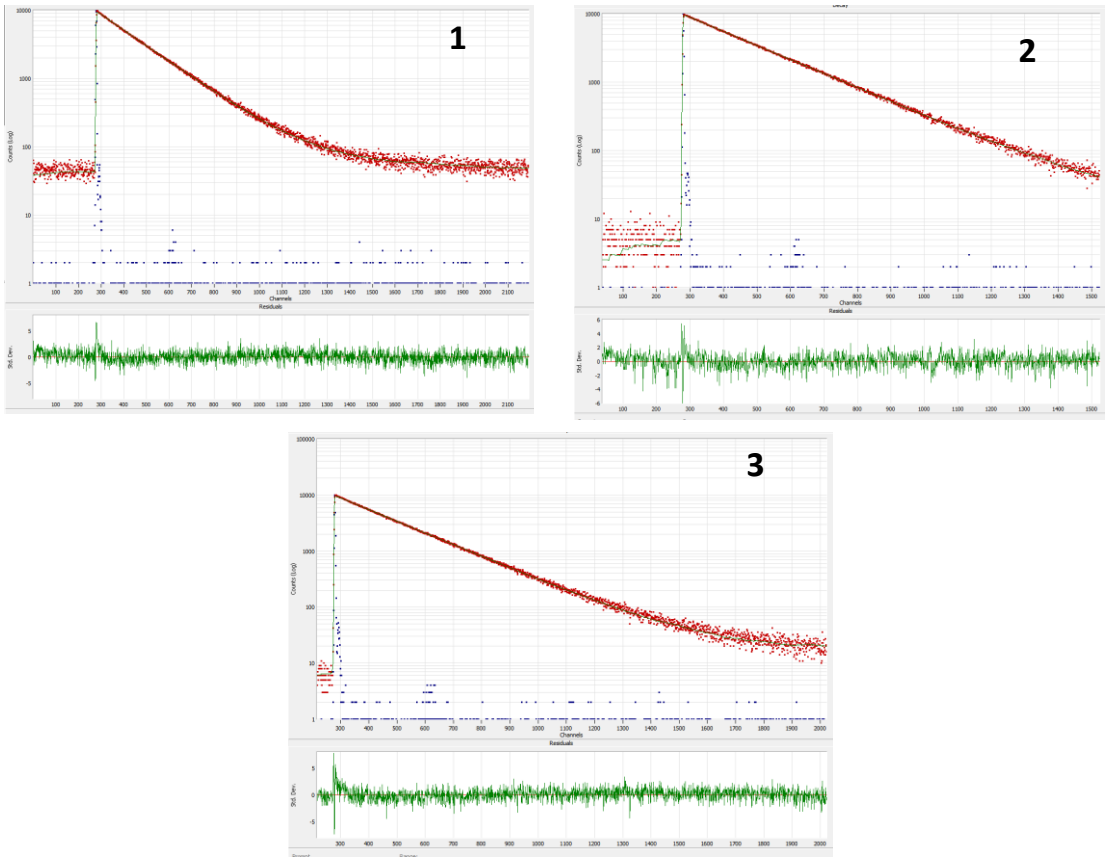

Figure S19. Photoluminescence decay curves of complexes **1–3** in CH_2Cl_2. λ_{ex} = 370 nm; λ_{em} = 626 nm.

Comments on the solid-state emission decay acquisition. Regarding the collection of data on solid samples, the spectrofluorimeter used has a flow: the decay is dominated by an artifact, which generates a signal in the µs range. We could not fix this problem, but measurements were done on many closely related complexes, the emission decay of which had been previously measured on a properly working apparatus by our collaborators in the ENS of Paris Saclay (see refs. 13 and 14, for example). If the long lifetime is not considered, the results were very close. Fitting with two exponentials is enough to obtain satisfying χ^2 values. Of course, the χ^2 values are improved when fitting with three exponentials. In this case, a short lifetime appears, the contribution of which is about one tenth of the contribution of the emission due to the complexes, and very minor with respect to the whole signal. According to the difficulties encountered in data recording, it seemed reasonable to consider only the results of the two-exponential fitting.

Table S6. Results of the emission decay measurements of the complexes **1**-**3** in the solid state (pristine and ground powders). Luminescence decay times (τ_i) with their respective fractions of intensity (f_i) defined by the multiexponential analysis of the decay curves: $I_F(t) = \Sigma a_i \times \exp(-t/\tau_i)$ and $f_i = a_i \times \tau_i/(\Sigma a_j \times \tau_j)$ where a_i is the normalized pre-exponential factor.

Complex		τ_1	f_1	τ_2	f_2	χ^2
1	Pristine	190	5.43	1255	94.57	1.11
	Ground	220	17.05	1141	82.95	1.21
2	Pristine	188	5.38	1400	94.62	1.07
	Ground	219	13.43	1415	80.25	1.17
3	Pristine	204	6.49	2385	93.51	1.17
	Ground	224	22.05	1718	77.95	1.28

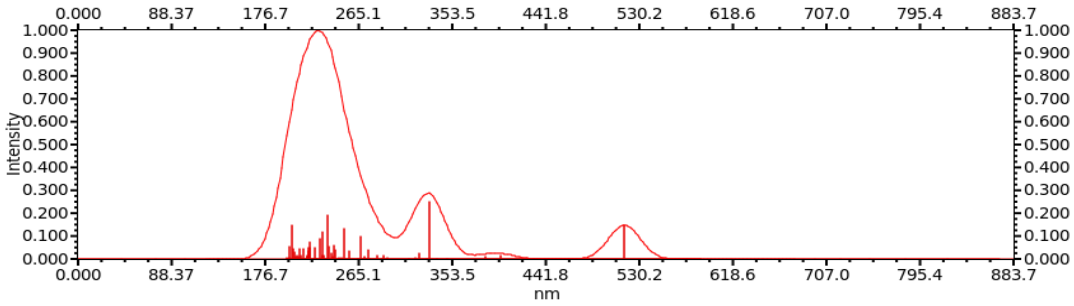

Figure S20. Theoretical UV-vis absorption spectrum and main electronic transitions for complex **1** calculated considering the crystal geometry and using the TD-DFT method at the PBEO/LANL2DZ level.

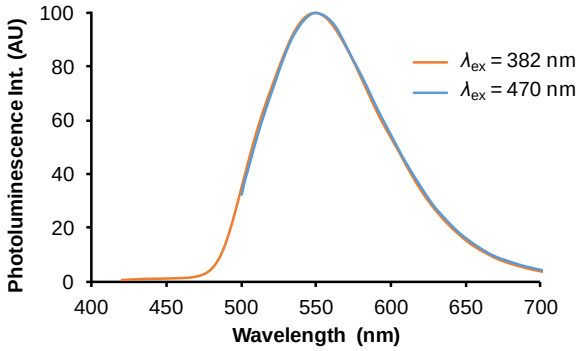

Figure S21. Normalized emission spectra of complex **3** as pristine microcrystalline powder, with excitation at 382 nm (orange line) and 470 nm (blue line).

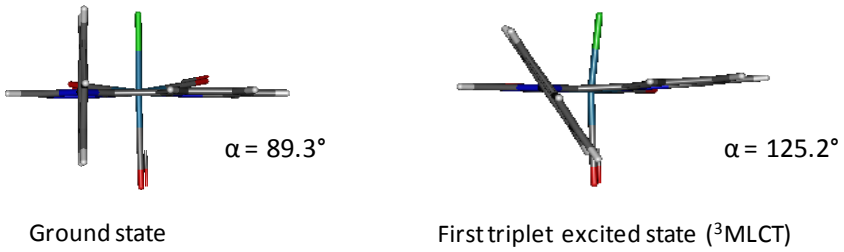

Figure S22. Geometry and phenyl-pyta dihedral angle value of complex **1** in the ground and first triplet excited state.

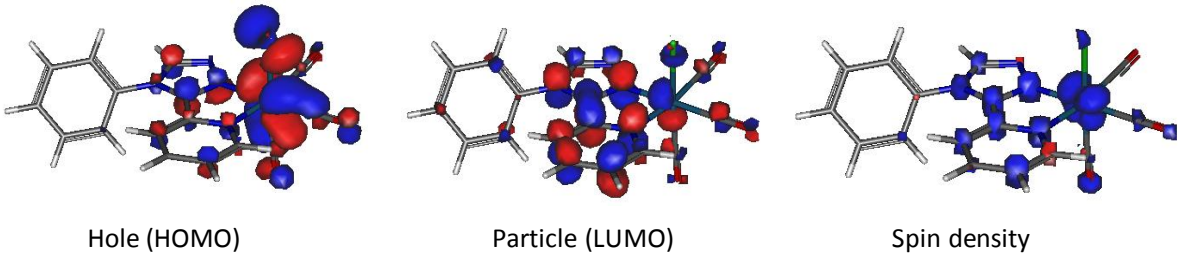

Figure S23. Graphical representation of the triplet excited state spin density of **1**. The isodensity plots are calculated for isovalue of 0.03 eV.

Fluorescence microscopy

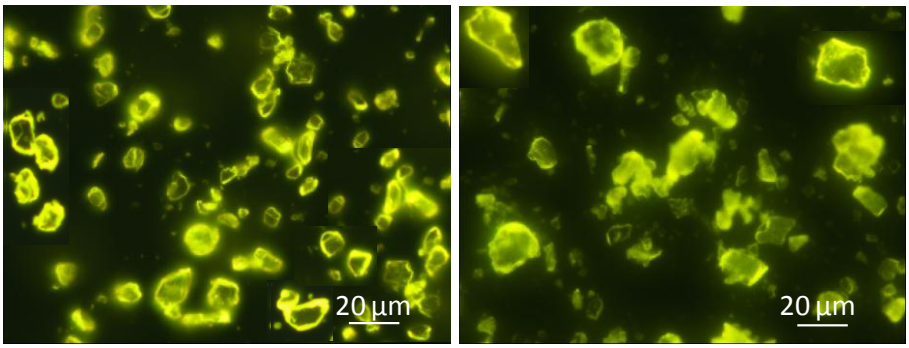

Figure S24. Fluorescence microscopy images of crystals of complexes **1** (a) and **2** (b). λ_{ex} = 450-490 nm, λ_{em} >500 nm.

NMR

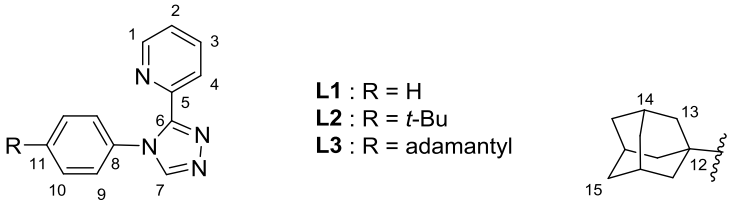

Figure S25. Carbon numbering for attribution of ^{1}H and ^{13}C NMR chemical shifts.

Figure S26. NMR spectra of complexes **1-3** in solution.

^{1}H NMR spectrum of complex 1 in $CDCl_3$

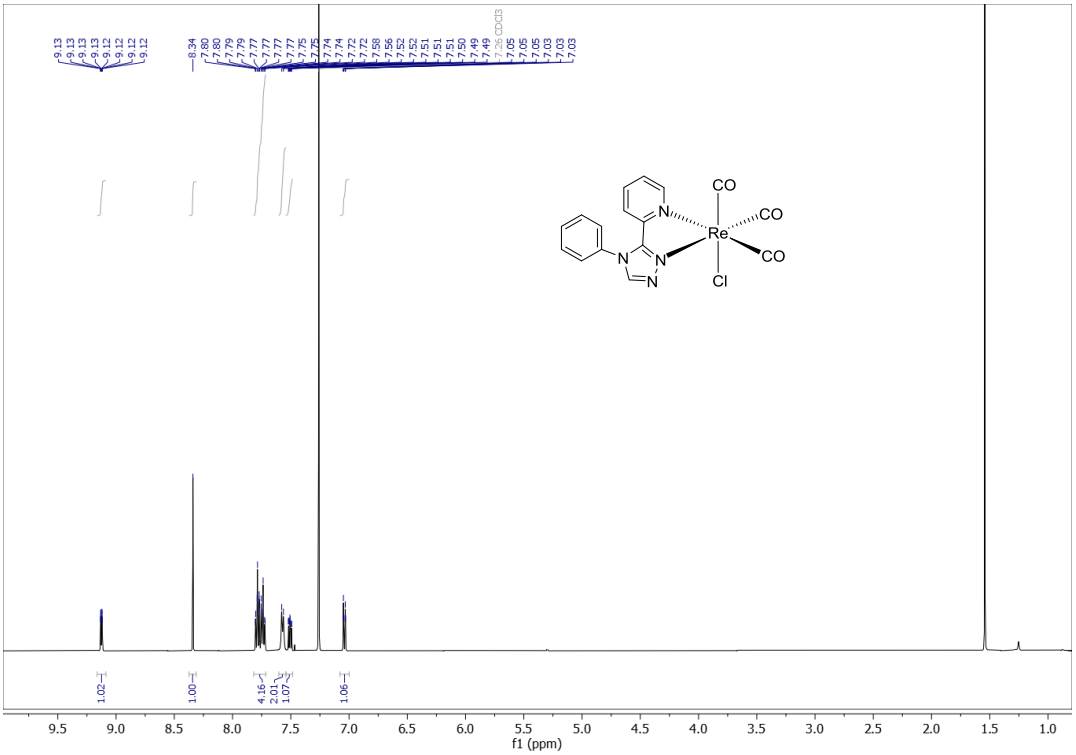

^{13}C NMR spectrum of complex 1

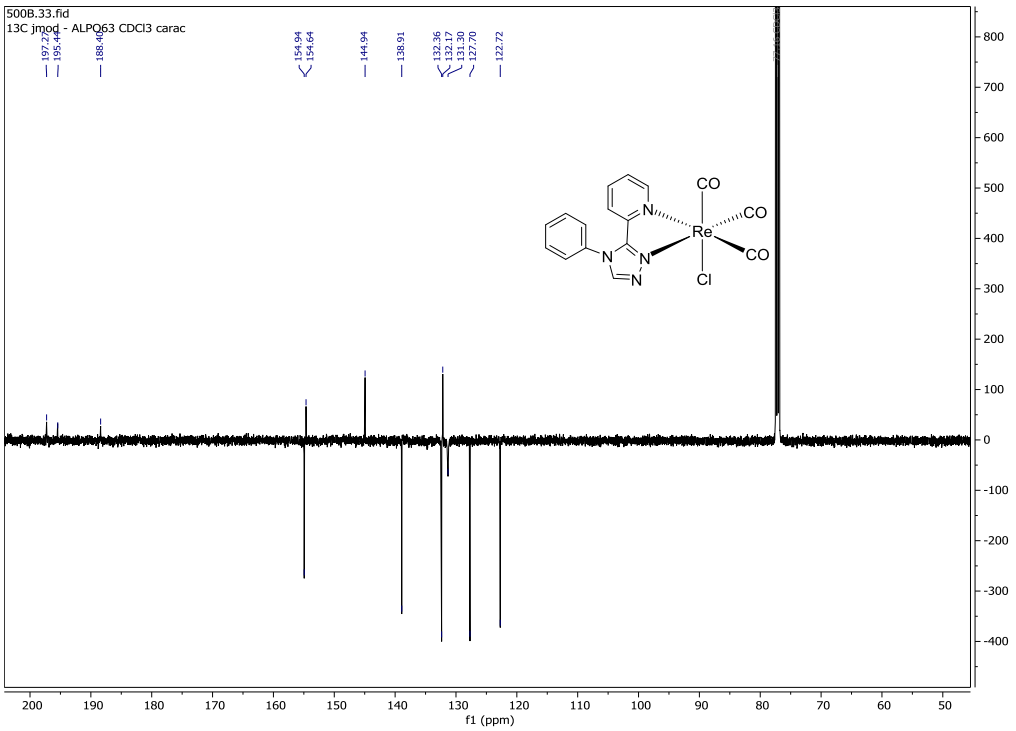

HSQC ^{1}H-^{13}C 2D NMR spectrum of complex 1 in $CDCl_3$

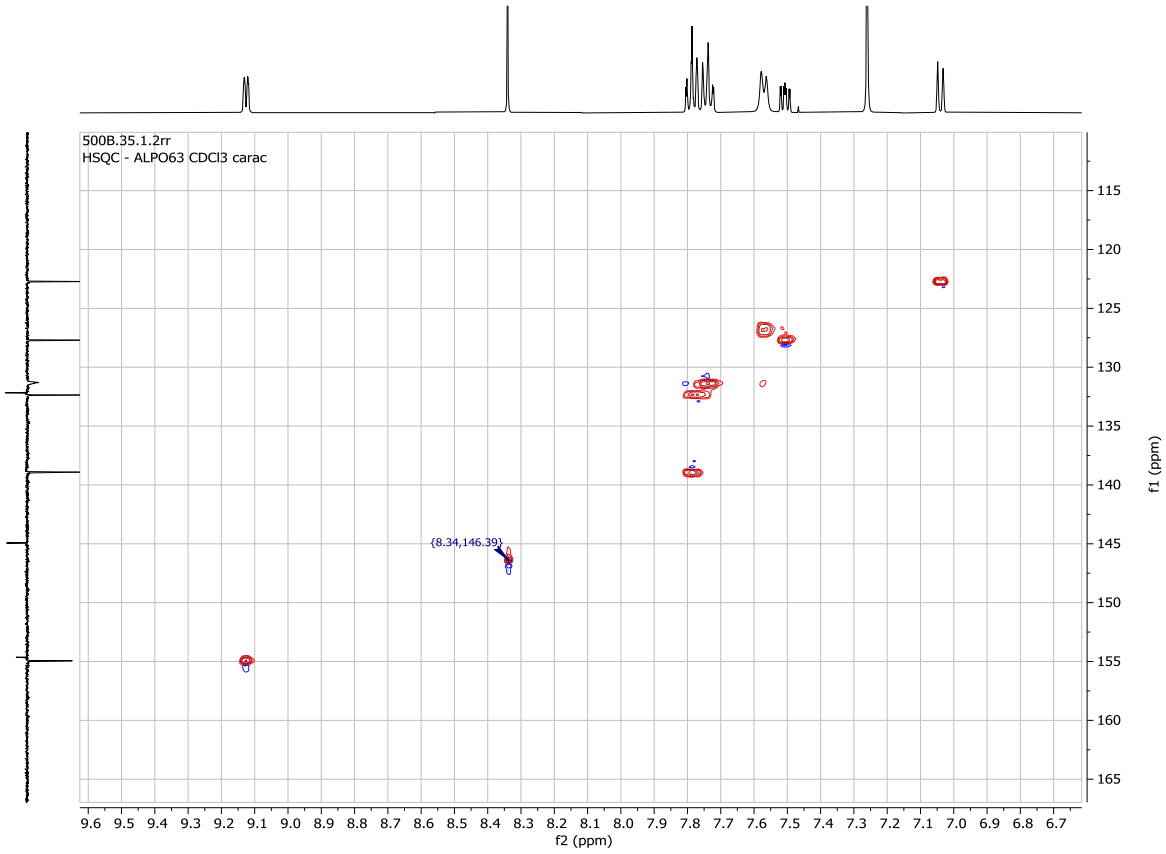

^{1}H NMR spectrum of complex 2 in $CDCl_3$

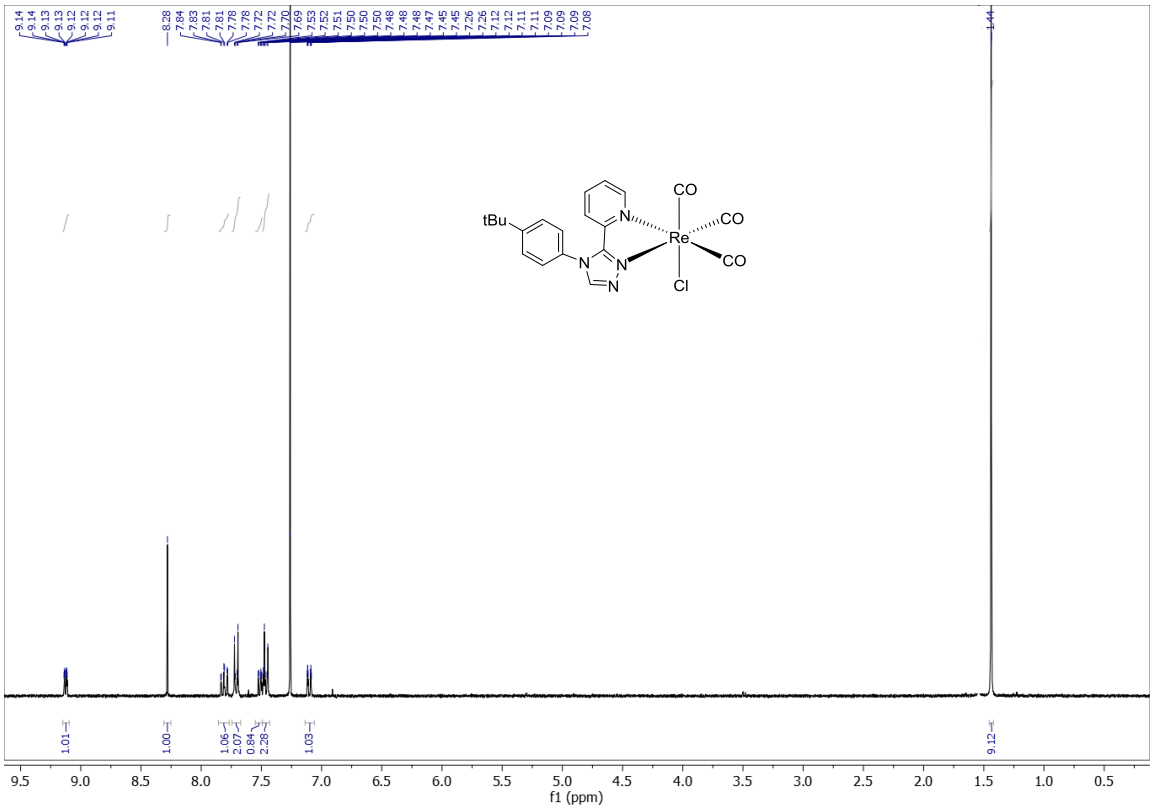

^{13}C NMR spectrum of complex 2

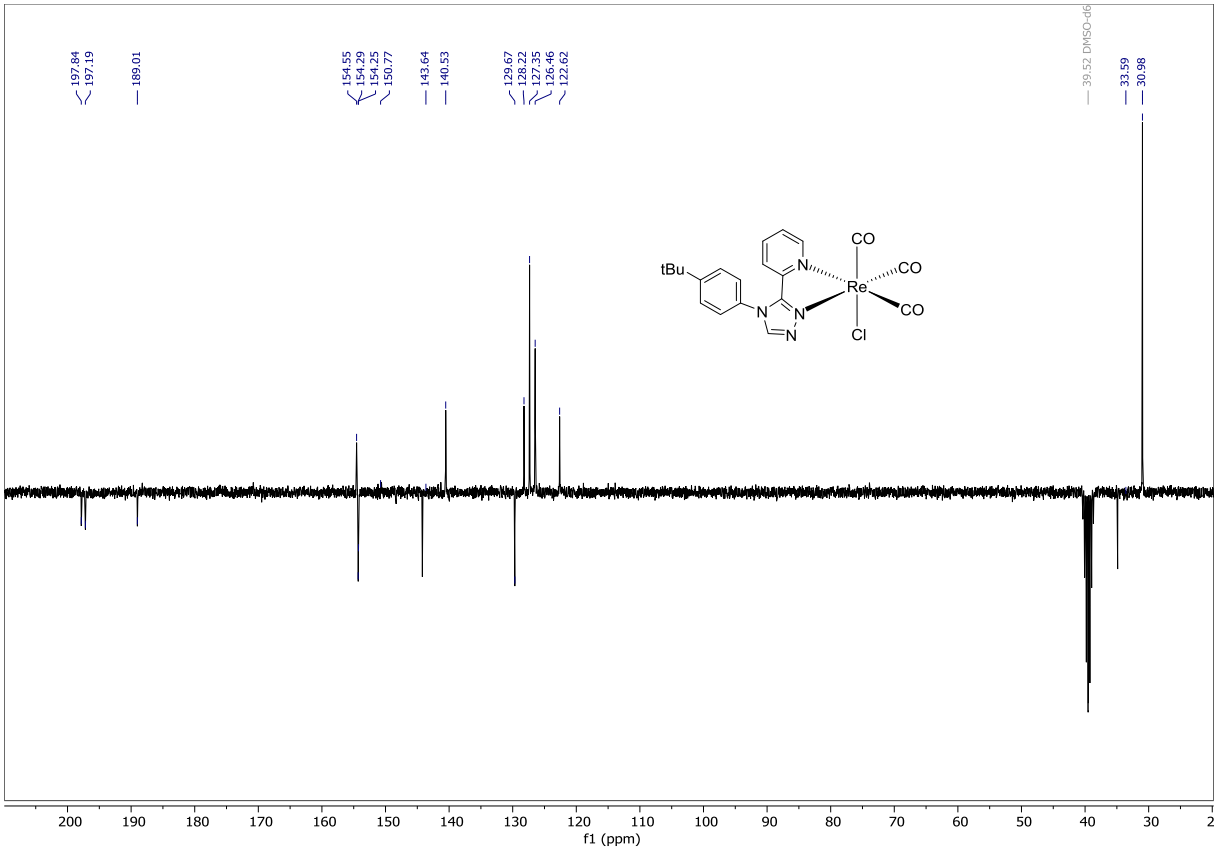

HSQC ^{1}H-^{13}C 2D NMR spectrum of complex 2 in DMSO-d6

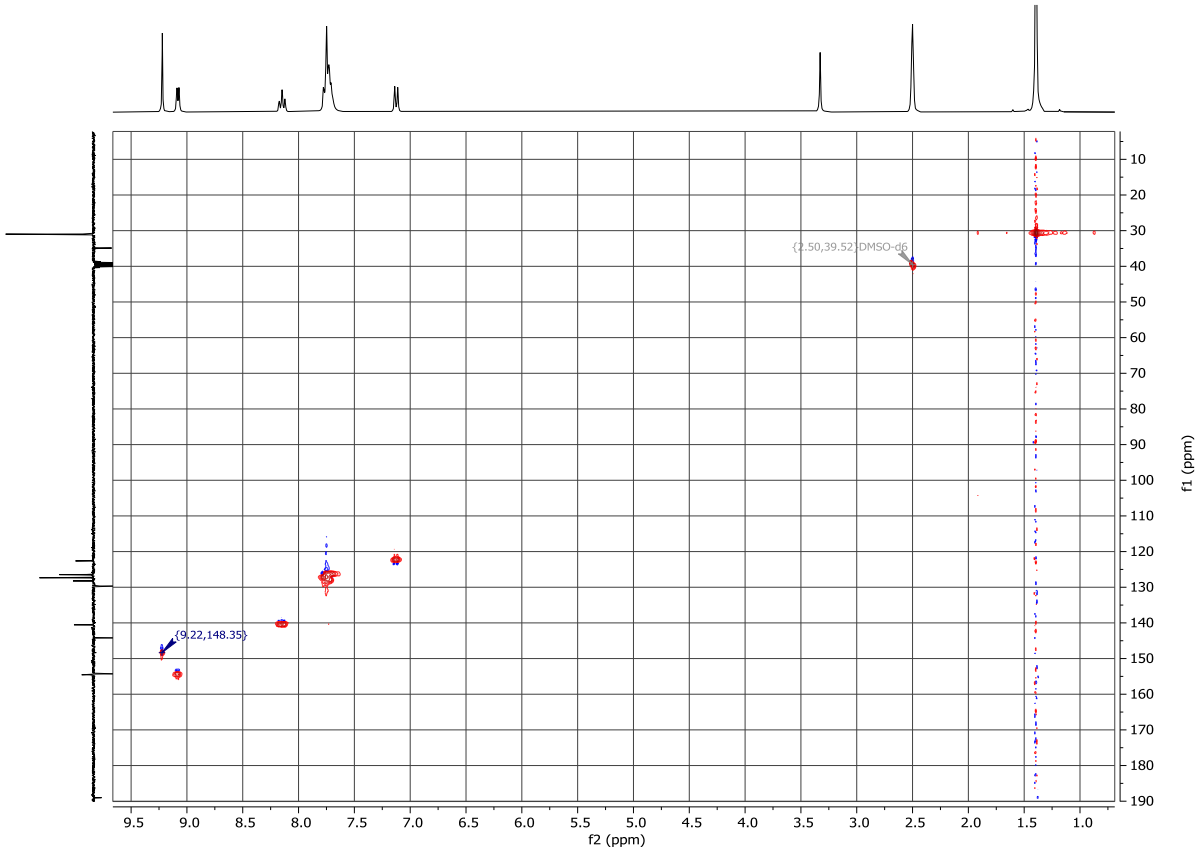

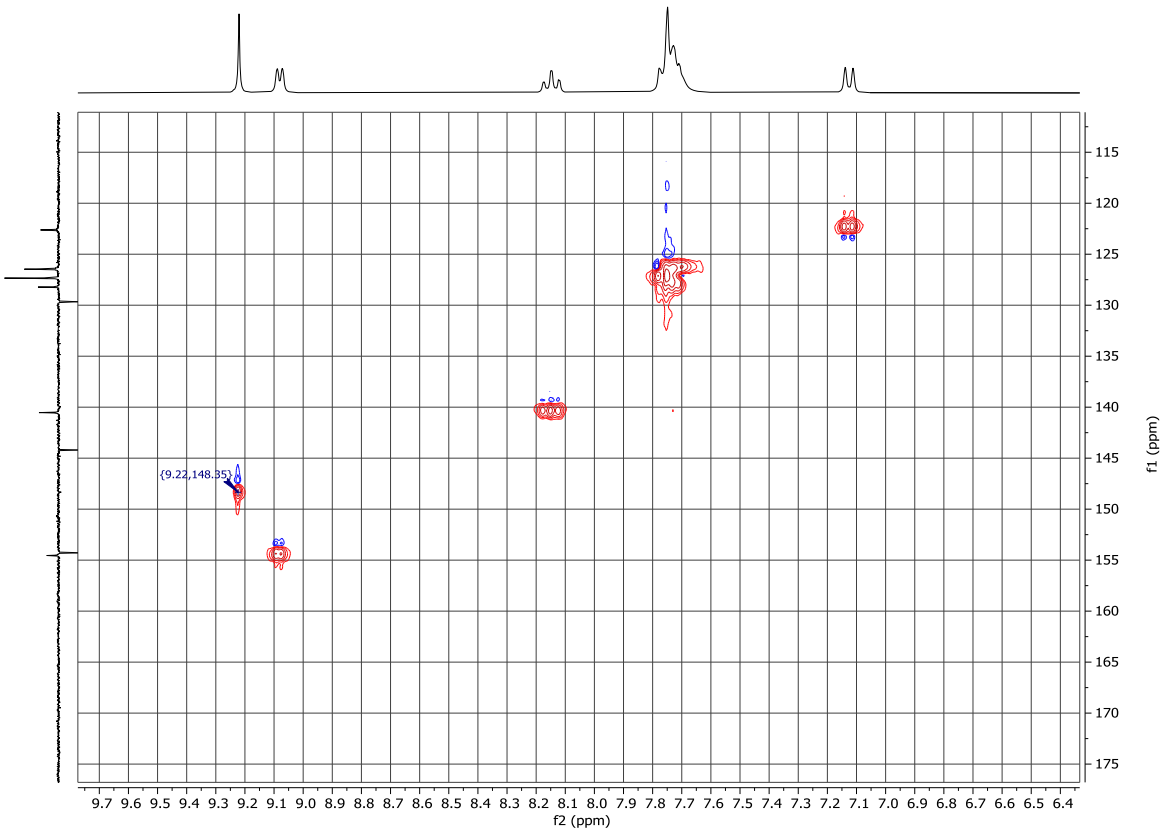

^{1}H NMR spectrum of complex 3 in $CDCl_3$

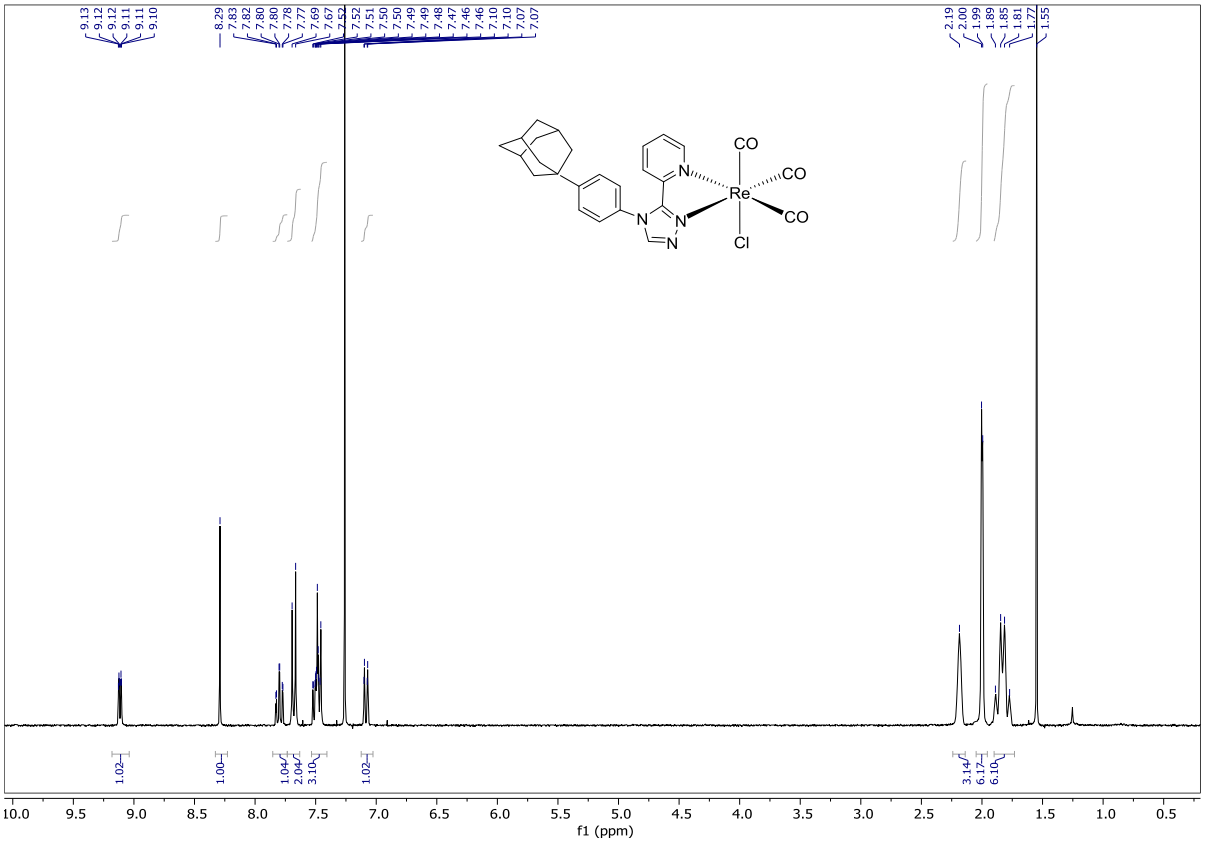

^{13}C NMR spectrum of complex 3

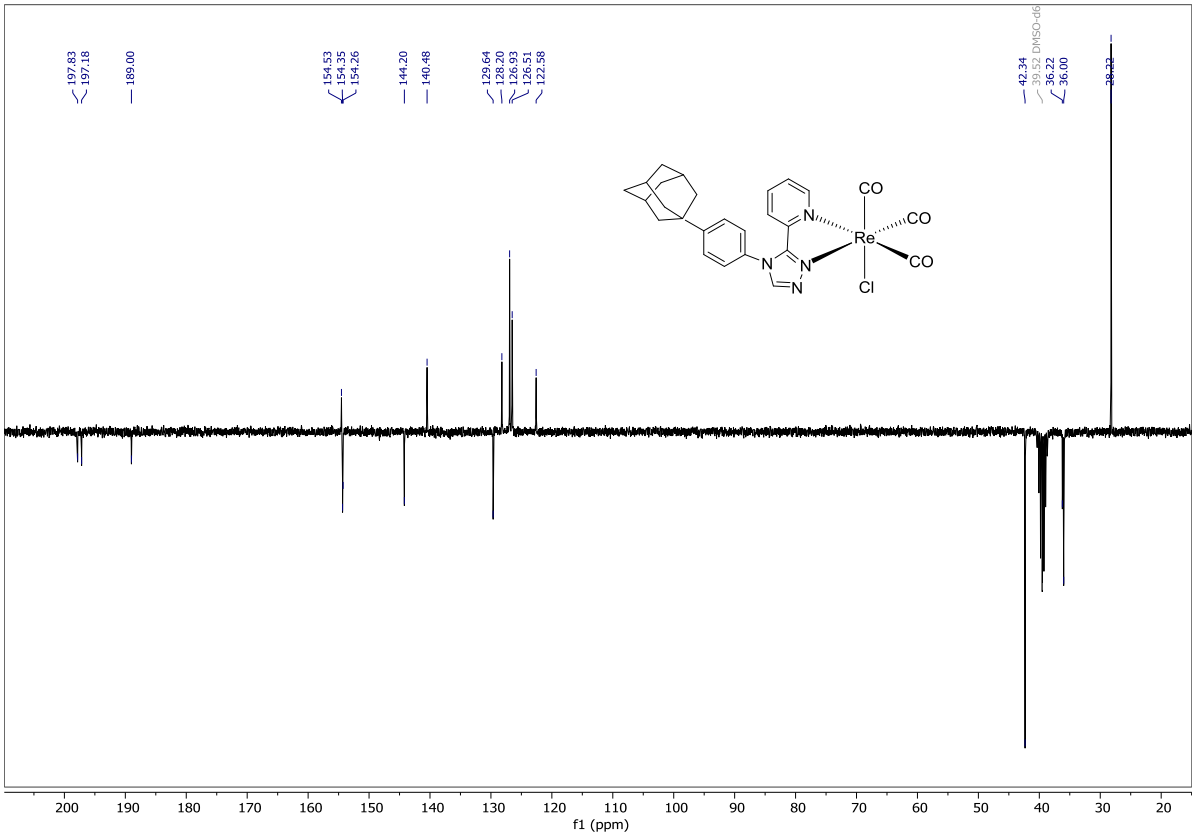

HSQC ^{1}H-^{13}C 2D NMR spectrum of complex 3 in DMSO-d6